239

Egypt. J. Chem. **Vol. 67**, No. 5 pp. 517 - 527 (2024)

Non-Ionic Polymeric as Acid Corrosion Inhibitor Surfactants of Fatty-Polyethylene Glycol-L-Cysteine

Mohamed A. Abbas [a*], Ahmed I. Adawy[b], Amr S. Ismail[b], Ibrahim M. Nassar[a]

[a*]*Petroleum Applications Department, Egyptian Petroleum Research Institute, 11727 Nasr City, Cairo, Egypt.* [b] *Petrochemicals Department, Egyptian Petroleum Research Institute, 11727 Nasr City, Cairo, Egypt*

Abstract

The current research deals with the elaboration of new non-ionic polymeric surfactants of fatty-polyethylene glycol-L-cysteine composites. Two saturated fatty acids, namely capric acid (CA) 'decanoic acid' and lauric acid (LA) 'dodecanoic acid', were experimentally employed to react with polyethylene glycol 600 (PEG 600) to produce main ester linkages. Otherwise, cysteine 'proteinogenic amino acid' was reacted with PEG 600 to produce thiol side chain structure. The obtained non-ionic polymeric surfactants, capriate L-cysteinate polyethylene glycol (Ib) and laurate L-cysteinate polyethylene glycol (IIb), having dual hydrophilic–hydrophobic sites. The characteristics of the prepared non-ionic surfactants were investigated using several spectroscopic techniques. Surface tension and thermodynamic behaviour as a function of concentration of the designed structures were assigned. The structure IIb that include a taller hydrophobic chain expresses extra surface activity especially at 70 °C comparing with structure Ib, it gives critical micelle concentration (CMC) 1.6×10^{-3} mole/liter and effectiveness 28.1 mN/m while the standard free energies of adsorption and micellization $\Delta G°_{ads}$ -62.3 and $\Delta G°_{mic}$ -18.3 KJ/mole. Polarization plots exhibited that both fatty composites were mixed–type corrosion inhibitors. At 10^{-2} M, the maximal inhibitory efficiencies of Ib and IIb were determined to be 92% and 93%, respectively. It is found that these prepared composites act as significant corrosion inhibitors and their protection actions proceed the order: IIb>Ib, and they mainly consist of the nature of the component. A morphological characteristic of carbon steel surface prior and next to acidic medium attack is screened. High-resolution features of the corrosion output assured the preservation given by fatty based non-polymeric surfactants on the metal surface exposed to acid solution.

Keywords: Non-ionic surfactant; Fatty acid; Polyethylene glycol; Cysteine; Corrosion inhibitor

1. INTRODUCTION

In the recent decades, non-ionic surfactants have accelerated their global proportion to achieve a good rank among the total surfactant fabrication processes [1,2]. Broadly, chemical structure of non-ionic surfactants has a wide variety of oxygen-containing hydrophilic functional sites and the number of hydrophobic moieties is limited [3]. Based on their properties, the non-ionic surfactants are electrically neutral compounds in which do not release any ions in aqueous media [4]. These components can produce several molecular weight compositions in solution without charge in their polar heads [5]. Thus, the high performance of non-ionic surfactant structure is subordinate to the hydrophilic–hydrophobic equilibrium as well as to the geometrical skeleton [6]. Furthermore, one of the most important ecological troubles like corrosion attacks of metallic surfaces especially steel is the major challenge in several global research studies. The degrading offensive of

acidic ambience on iron-based substances causes expensive costs [7]. Sundry preservation procedures like electrochemical coating [8,9], anodic/cathodic protection [10], oxidizing process [11] and inhibitor adsorption [12] have been employed to eliminate the steel attack. Corrosion inhibitors are chemical components that typically hold, diminish, or prohibit interactions between steel metal surface and ambient solutions, when embedded in aggressive fluid in extremely small ratios [13,14]. Long chain surfactants are utilized in a broad diversity of implementations in which extent and distribution of linkage equilibrium of surfactant composition must be harmonious with the chain length of other components exist in the structure [15].

These significant combinations modify their attitudes and molecular interactions which in turn stabilize adsorption of surfactant species on metal surfaces [16]. Newly, employment of non-ionic composites against corrosion attack has concerned as significant steel protectors. Efficiency of corrosion inhibitor adsorption

through their polar head sites depends on metal nature, surfactant composition, inhibitor concentration, temperature, and pH range and exposure period [17]. Raising the concentration elevates the corrosion inhibition efficiency. Moreover, polymeric structures with longer non-ionic chain length reveals higher corrosion inhibition performance [18]. As compared to cationic and anionic surfactants, non-ionic surfactants have more environmentally friendly influence, more cost-effective and can be easily mixed without the risk of instability or precipitation action. The solubility of non-ionic surface active agent is not good like ionic surfactants, however they do not change the pH of the solution [19]. Moreover, ionic surfactants are highly cost due to the high-pressure hydrogenation process which occurred throughout their synthesis procedures. Wherefore, the non-ionic surfactant became the better alternative for the modern corrosion inhibition technique [20].

In the current research, a new combination of water soluble polymeric non-ionic surfactant containing fatty acids-polyethylene glycol-L-cysteine was reported. The studied non-ionic polymeric surfactants, capriate L-cysteinate polyethylene glycol (Ib) and laurate L-cysteinate polyethylene glycol (IIb) structures, the present study not only looked investigated as potential inhibitors of corrosion however, additionally they were investigated to developed the surface tension characterization. The steel corrosion inhibition influence of the prepared two ester compounds; capriate L-cysteinate polyethylene glycol and laurate L-cysteinate polyethylene glycol were categorized as (Ib) and (IIb) correspondingly, as shown in Fig. 1, on the metal samples in aqueous acidic medium using fundamental electrochemical and thermodynamic techniques. Additionally investigated were the inhibitor components' reactive effects and the concentration ratio's impact on the efficiency of corrosion control.

Before and after the corrosion tests, the carbon steel superficies were inspected using a variety of spectroscopic techniques, including FTIR, XRD, EDAX, and SEM.

2. EXPERIMENTAL
2.1. Materials
The materials, solvents and reagents such as capric acid, lauric acid, polyethylene glycol 600, L-cysteine, xylene, petroleum ether and p-toluene sulphonic acid were acquired from Sigma-Aldrich chemical company and were applied with no extra purifications.
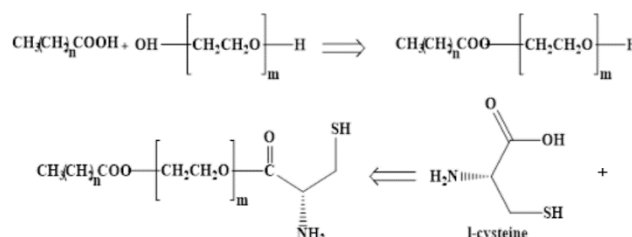
2.2. Fabrication of non-ionic surfactants
Polyethylene glycol (PEG) 0.1 mole, Mwt =600 was esterified by equimolar of capric acid and lauric acid ("CH_3 $(CH_2)_8COOH$" and "CH_3 $(CH_2)_{10}COOH$") respectively in (150 mL) of xylene. Posteriorly, a 0.01% p-toluene sulphonic acid was introduced into the admixture as a catalyst. The esterification reaction was proceeded inadequate heating system (140 ^{o}C) and awaiting for the amount of water produced from esterification to get rid of it. Thereafter, the solvent (xylene) was withdrawn from the blend using vacuum rotary evaporator technique as well as the catalyst (p-

toluene sulphonic acid) was gathered from utilizing petroleum ether. As a consequence, filtration process was carried out through standard vacuum distillation methods to evacuate the remains and residual species [21]. The synthesized combination which was remarked as Ia and IIa, for capriate PEG and laurate PEG, respectively.

2.3. Preparation of L-cysteine based capriate PEG (Ia) and laurate PEG (IIa)

0.1 mole of polyethylene glycol alkanoates (Ia and IIa) were esterified by equimloar of L-cysteine in xylene (150 mL). Ptoluene sulphonic acid (0.01%) was introduced into the mixture as a catalyst. The reaction was accelerated under effect of heat (140 ^{o}C) waiting for the amount of azeotropic water produced from esterification to get rid of it. After that, the solvent was extracted using a vacuum. The catalyst was taken out of the mixture using petroleum ether. Afterwards, the filtration procedure was finished using vacuum distillation techniques to get rid of any durable and leftover components. The obtained two ester compounds; capriate L-cysteinate polyethylene glycol and laurate L-cysteinate polyethylene glycol were classified as (Ib) and (IIb), respectively, as shown in Figure 1.

Fig. 1 Preparation of Nonionic surfactants based on PEG (M.wt. = 600): n = 8, decanoate -L-cysteinate polyethylene glycol (Ib) and n=10, laurate - L-cysteinate polyethylene glycol (IIb).

Spectroscopic analysis

Several spectroscopic procedures were employed such as Fourier transform infrared spectroscopy (FT-IR) utilizing ATI Mattson form Genesis Series (USA) infrared spectrophotometer adopting KBr technique. X-ray diffraction (XRD) models were performed at 40 KV and 40 mA in the scope $2\theta = 4\text{-}80°$, utilizing Philips Powder Diffractometer with Cu Kα1 radiation. The apparatus was managed. The spectra were adjusted at scanning speed of $2°$ in 2θ/min. The morphology was studied using scanning electron microscope (SEM, model Jeol 5410).

2.4. Surface active characterization
By surveying their attitude in aqueous solutions, the tension-active features of the two constructed formulas were assessed.

2.4.1. Surface tension
Using a Kruss type 6 Du-Nouy Tensiometry, data was collected for the designed non-ionic polymeric surfactants (Ib and IIb) system at various temperatures (40, 50, 60, and 70 ^{o}C) with concentrations that range from 4×10^{-2} to 1.9×10^{-5} M/L.

2.5.2. Surface criteria

a) Critical micelle concentration (CMC)

Surface tension method was used to settle the fabricated surface active agent. Results of the surface tension calculations were presented against the corresponding ratios. As the CMC fixations change, so does the break in the SC charts.

b) Effectiveness (π_{CMC})

The difference between the surface tensions of the surfactant solution (γ) and pure water (γo) at the critical micelle concentration is known as πCMC.

πCMC is equal to $\gamma_o - \gamma_{CMC}$.

c) Efficiency (Pc_{20})

The concentration (mol/liter) of Surface active agent solutions capable of reducing surface tension by 20 dyne/cm is known as Efficiency (Pc20).

d) Maximum surface excess Γ_{max}

The results of the largest surface excess Γ_{max} calculated using the Gibbs equation from surface or interfacial data. [22].

$\Gamma_{max} = -1 / 2.303\ RT\ (\delta\gamma / \delta \log C)_T$

Where, Γ_{max} is maximum surplus surface area in mole/cm^2, R is universal gas constant 8.31×10^7 ergs mole^{-1} K^{-1}, T is absolute temperature (273.2 + $^{\circ}$C), $\delta\gamma$ is surface pressure in dyne/cm, C is surface active agent concentration and $(\delta\gamma/ \delta \log C)_T$ is the slope of a surface tension vs. log concentration chart at a fixed temperature plotted beneath CMC.

e) Minimum surface area (A_{min})

Each fragment's zone at the interface allows information about the loading grade and the adsorbed surfactant fragment's path to be entered. The mean zone, expressed in square angstroms, that is necessary for each individual molecule adsorbed on the interface [23] can be determined using:

$A_{min} = 10^{16} / \Gamma_{max} N$

A_{min} is Minimum surface area in $^{\circ}$A^2, Γ_{max} is Maximum surface excess in mole /cm^2, and N Avogadro's number 6.023×10^{23}

f) Thermodynamic criteria of micellization and adsorption:

Gibb's adsorption equations were utilized to estimate the criteria of the two developed nonionic surfactants, as indicated below:

$\Delta G^O_{mic} = RT \ln (CMC)$

$\Delta G^O_{ads} = \Delta G^O_{mic} - 6.023 \times 10^{-1} \times \pi_{CMC} \times A_{min}$

$\Delta S_{mic} = -d (\Delta G^O_{mic}/ \Delta T)$

$\Delta S_{ads} = -d (\Delta G^O_{ads}/ \Delta T)$

$\Delta H_{mic} = \Delta G^O_{mic} + T \Delta S_{mic}$

$\Delta H_{ads} = \Delta G^O_{ads} + T \Delta S_{ads}$

where (ΔG^o_{mic}) free energy of micellization: the work of transfer of surfactant molecules to the bulk of a solution to form micelles, (ΔG^o_{ads}) free energy of adsorption: the work of transfer of surfactant molecules from the bulk of a solution to the surface, (ΔS_m) entropy: the degree of disorder in the system in micellization, (ΔS_{ads}) entropy: the degree of disorder in the system in adsorption, (ΔH_m) enthalpy: total heat content of the system in micellization process, (ΔH_{ads}) enthalpy: total heat content of the system in adsorption process.

3. RESULTS AND DISCUSSION

3.1. Structural Investigations

FTIR diagrams of the synthesis non-ionic polymeric surfactants; capriate L-cysteinate polyethylene glycol (Ib) and laurate L-cysteinate polyethylene glycol (IIb) are approximately comparable.
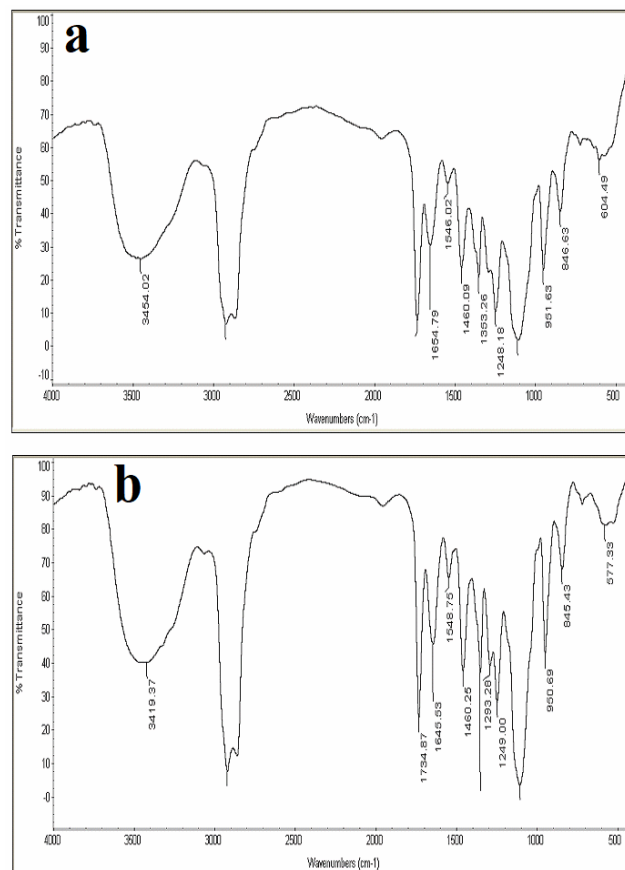

Fig. 2 FTIR of Nonionic polymeric surfactant (a) Ib and (b) IIb compounds.

From Fig. 2, it is clearly seen that several absorption bands, like the bands at 2923.08–2923.59 cm^{-1} is owing to asymmetric C-H vibrations as mentioned before [24], while the bands at 1734.87-1735.71 cm^{-1} is related to ester groups (-COO-). The N-H bending spectra were observed in 1645.53-1654.79 cm^{-1}. The bending spectra of CH$_2$ around 1460.09–1460.25 cm^{-1} and a number of spectra around 1400–1200 cm^{-1} were given to the bending C-H and O–H. whereas the broad bands around 3419.37–3454.02 cm^{-1}, stretching O-H of free COOH [25].

3.2. Tensiometric parameters

Using a surface tension method, the proposed non-ionic polymeric surface activeagent (Ib) and (IIb) were screened as surfactants by determining the surface tension of their media at various temperature ratios: 40, 50, 60, and 70 $^{\circ}$C. The findings are displayed in Fig. 3. It is well known that a significant decrease in surface tension occurred as a result of an increase in the concentration of the intended surfactants, which were deduced from the

mobility of the surface active agent particles toward the interface from the majority of the mixture. [26].
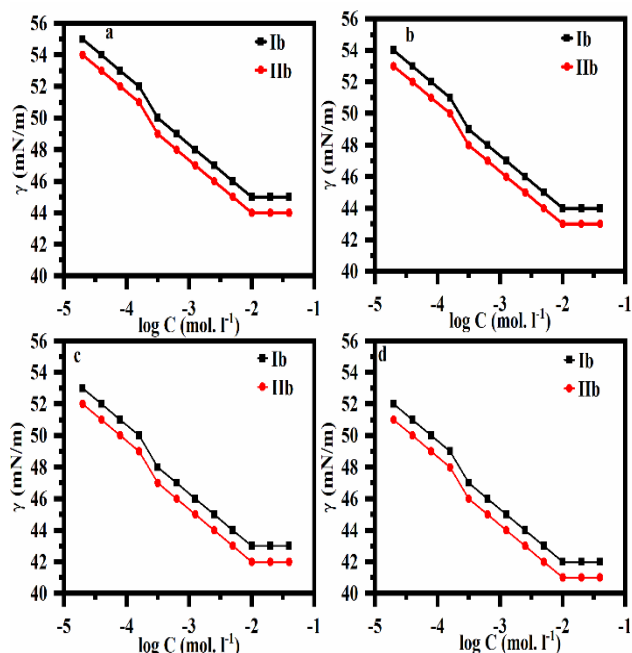
Fig. 3 Surface tension vs. log Concentration of synthesized polymeric surfactants (a) Ib and (b) IIb compounds at: (a) 40 ^{o}C, (b) 50°C, (c) 60°C, (d) 70°C.

Primarily, the surface tension drop of the surfactants at the equivalent content is significantly influenced by the hydrophobicity of the proposed structures under investigation. In order to maximize hydrophobicity and show further deviation between the polar system and the hydrophobic sites due to their opposite polar nature, structure IIb, which includes a taller hydrophobic chain, expresses extra lowering in the surface tension when compared to structure Ib. This was explained based on a grand trend of the more hydrophobic design.

Moreover, a decrease in surface tension was observed when temperatures rose from 40 to 70 ^{o}C. This was caused by the hydrophilic portions drying up, which reduced the solubility of the surfactant molecules that were rising to the surface. CMC values were calculated for the intended surfactants at a range of temperatures, including 40, 50, 60, and 70 oC. Interception of the micellar patterns at particular breakpoints corresponding to the content range denoted by a linear reduction in surface tension and the near-constant surface tension concentration zone (γ); Table 1. The fact that nearly all of the surfactant media's physicochemical characteristics exhibit unexpected behavior at this ratio makes the CMC values a serious concern. Undoubtedly, the CMC results indicate a decrease when the hydrophobicity of the surfactant components is increased. This is because the increased hydrophobicity of the Micelles forms at the saturation level when surfactant components decrease their dissolution and concentrate inhibitor particles on the surface.

Table (1): Surface properties of polymeric surfactants at 40, 50, 60, 70 °C.

Temperature .	Surfactant	CMC X 10^{-3}, Mole/liter	π_{CMC}, mN/m	Pc$_{20}$ X 10^{-5}, Mole/liter	Γ_{max} X 10^{-11}, Mole/cm^2	A$_{min}$, nm^2
40 °C	Ib	3.2	25.3	15	6.1	2.7
	IIb	3	26.3	7.9	6.2	2.6
50 °C	Ib	2.8	26.2	7.9	6.2	2.6
	IIb	2.4	27	4	6.3	2.6
60 °C	Ib	2.2	26.8	4	6.4	2.5
	IIb	2	27.7	2	6.5	2.5
70 °C	Ib	1.8	27.5	2	6.6	2.5
	IIb	1.6	28.1	1.6	6.7	2.5

On the other hand, as the temperature rises, the CMC decreases because the hydrophilic moieties that support micellization are less hydrated. On the other hand, when the temperature rises and micellization is disliked, chaos is seen in the regular water molecules that surround the hydrophobic moieties. Table 1 shows that when the temperature increased, the micellization improved as a result of the CMC. The CMC data also demonstrate the designed surfactants' capacity to get dissolved in water; structure IIb showed the lowest CMC values, indicating a development in its solubility [27]. As a result, increasing the hydrophobicity of the engineered surfactants encourages the interface's surface tension to be reduced, which increases efficacy but decreases efficiency (P$_{C20}$), or the amount of surfactant required to get a 20 mN m^{-1} depression in surface tension. The surface tension of the surfactants solution at the CMC specifies the influence. At this point, the term "surfactant content" refers to the lowest concentration required to achieve the best adsorptive effect.

The maximum surface excess, or Γ_{max}, is a crucial metric for assessing the surface behavior of the engineered surfactant fragments at the interface, which can be screened by increasing the hydrophobicity and using the Gibbs adsorption isotherm. As the adsorption tendency of the surfactant fragments at the surface grows, the maximum surface excess values at the interface also grow, indicating a highly developed surface concentration. Once the surface adsorption was fully occupied, the designed nonionic components are dealt with by the minimal surface area Amin, (nm^2) addresses the designed nonionic components when the surface adsorption is fully occupied. Raising the amount of adsorbed particles at the interface causes the scores of the most surface over flow to enlarge, which may lead to a decrease in the area reachable for each molecule. The minimum surface area (A$_{min}$) is one of the primary records regarding the orientation type of the surfactant fragments at the interface. Table 1 displayed the values of CMC, π_{CMC}, P$_{C20}$, Γ_{max}, and A$_{min}$. To put it succinctly, it is evident that structure IIb, when compared to the other synthesized structure, attained the desired surface tension results at a modest concentration. Consequently, structure IIb may be considered to have considerably finer surface features and a higher tensio-activity than structure Ib [28].

3.3. Thermodynamic of micellization and adsorption:

The designed surfactants in the solution were subjected to thermodynamic behavior analysis using the values of ΔG°_{ads} and ΔG°_{mic} at 40, 50, 60, and 70 ºC. Tables 2 and 3 contain reports on the thermodynamic characteristics of adsorption and micellization. The tables clearly show that the designed surfactants' standard free energies for micellization and adsorption have consistently negative values. The situation attested to the normal course of the micellization and adsorption processes. Additionally, the designed structures' thermodynamics of adsorption produced considerably lower scores when compared to the micellization values, confirming the adsorption route's great preference over the micellization one. Furthermore, because the adsorbed particles at the interface are densely packed, it is possible to explain the large discrepancy between ΔG°_{ads} and ΔG°_{mic} records by the fact that water molecules do not react strongly through them [29].

Table (2): Thermodynamic parameters of micellization of polymeric surfactants at 40, 50, 60, 70 °C.

Temperature	Surfactant	$\Delta G^{o}_{mis.}$ KJ/mole	$\Delta H^{o}_{mis.}$ KJ/mole
40 ºC	Ib	-14.9	43.1
	IIb	-15.1	-49.5
50 ºC	Ib	-15.8	-44.8
	IIb	-16.2	-51.7
60 ºC	Ib	-17.0	-50.2
	IIb	-17.2	-53.8
70 ºC	Ib	-18.0	-52.3
	IIb	-18.3	-56.1

*Table (3): Thermodynamic parameters of adsorption of polymeric surfactants at 40, 50, 60, 70 °C.*

Temperature	Surfactant	$\Delta G^{o}_{ads.}$ KJ/mole	$\Delta H_{ads.}$ KJ/mole
40 ºC	Ib	-53.0	-168.9
	IIb	-46.8	-360.0
50 ºC	Ib	-56.7	-176.4
	IIb	-56.8	-380.0
60 ºC	Ib	-58.9	-185.5
	IIb	-50.6	-440.0
70 ºC	Ib	-62.7	-193.0
	IIb	-62.3	-464.0

A system's total heat content is expressed in ΔH. Enthalpy change is the amount of heat that enters or exits a system during a reaction. An essential component in determining whether a reaction can occur is whether the system's enthalpy rises (when energy is added) or falls (when energy is released). The exothermic reaction (heat generation) is indicated by the negative values of ΔH_{mic} and ΔH_{ads}. More energy has been released into the environment following an exothermic reaction than was taken in to start and sustain the process.

## 3.4. Electrochemical Impedance Spectroscopy (EIS)

To describe the generated polymeric composites' protective function on the metallic surface, EIS was used. By identifying the typical kinetic interface between the steel and acid systems using Nyquist plots, this method was investigated. The corresponding open circuit was

appropriately matched to the Nyquist plots (Figure 4 (a, b)).
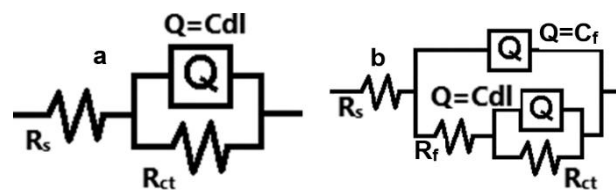
Figure 4 the equivalent circuit model used to fit the EIS data (a) for blank and small concentration (b) for high coccentration.

The carbon steel electrode's Nyquist plots with and without the fatty inhibitors following exposure to an acidic solution (Figure 5). The measurements that the fitted data was used to create are listed in Table 4. Where R_s solution resistance, R_f is the thin film resistance at high concentration from inhibitor, Q is the constant phase element (CPE), which is comparable to the thin film capacitance (C_f) and the double layer capacitance (C_{dl}), and R_{ct} is the charge transfer.
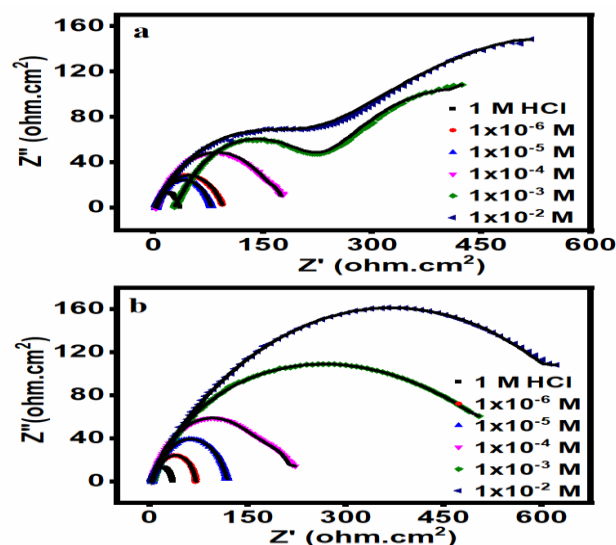
Figure 5 EIS Nyquist plot of the EIS data for carbon steel in 1.0 M HCl in absence and presence of different concentrations of (a) Ib and (b) IIb compounds.

Effective capacitive loops were evident in the Nyquist plots, as Figure 5 makes evident. The loop's highest value almost demonstrates the maximum resistance to corrosion. In presence of inhibitor, the loop diameter was greatly enlarged, and the steel in 1M HCl media was clearly protected by the high concentration of non-ionic inhibitors. This pattern indicates that the protection is improved by include more fatty inhibitors and by raising their content. Additionally, it is noted that, as shown in Table 4, the Q and their n values for the polymeric corrosion inhibitor represent double layer capacitors. The acquired results additionally demonstrated the presence of these inhibitors at increasing concentrations that reduce steel corrosion because of the metal surface's verified passivity behavior [30].

Table 4: The impedance parameters for different concentrations of C10 and C12 compounds at ambient temperature in 1 M HCl

| Inhibitor compound	Conc. (M)	R_s ohm.cm²	Q (S Sec^{n}m²) x10^{-5}	C_f	n x10^{-2}	R_{ct} ohm.cm²	Q (S Sec^{n}m²) x10^{-5}	n x10^{-2}	R_{ct} ohm.cm²	C_{dl} µF/cm²	α°	S	θ	%η_{Rct}
	1MHCl	3.1±0.1	-	-	-	-	74±6.1	84±1	32±0.6	362	-30	-0.20		
C10	10^{-6}	4.1±0.1	-	-	-	-	38±0.5	74±0.8	75±9	109	-45	-0.16	0.57	57
	10^{-5}	3.6±0.1	-	-	-	-	38±3	72±0.7	91±1.4	103	-46	-0.09	0.65	65
	10^{-4}	3.7±0.1	-	-	-	-	27±2.5	76±0.6	172±2.9	102	-46	-0.05	0.81	81
	10^{-3}	2.6±0.1	0.16±0.4	23	63±0.4	219±2.5	19±4.3	78±1.3	361±13	89	-46	-0.03	0.91	91
	10^{-2}	3.3±0.3	0.14±1.3	15	62±1	199±2.4	15±0.3	78±0.9	600±17	80	-46	-0.01	0.95	95
C12	10^{-6}	3.2±0.1	-	-	-	-	36±1.7	75±0.2	69±1.5	105	-47	-0.23	0.54	54
	10^{-5}	4.2±0.1	-	-	-	-	32±4	74±1	116±1.4	100	-48	-0.14	0.72	72
	10^{-4}	2.3±0.1	-	-	-	-	28±1.9	71±0.6	218±3.4	89	-49	-0.11	0.85	85
	10^{-3}	2.8±0.1	-	-	-	-	17±1.4	76±0.6	564±11	81	-49	-0.03	0.94	94
	10^{-2}	4.5±0.1	-	-	-	-	13±2	80±0.6	747±19	73	-52	-0.02	0.96	96

In this way, the film and charge transfer resistance (R_f and R_{ct}) and solution resistance (R_S) values were also raised. Additionally, because of the adsorption process of the polymeric inhibitor ingredients on the steel interface, the values of double layer capacitance (C_{dl}) reduced by the presence of inhibitor are connected with the processing of the double layer thickness[31]. Furthermore, the stability of the 'n' value in the range of 0.74–0.78 for Ib and 0.75–8.0 for IIb indicated that, both in the presence and absence of inhibitors, the kinetics of charge transfer track the dissolving of carbon steel in an HCl environment. The enhanced action of the inhibitor in an acidic media was demonstrated by the EIS measurement results acquired from the Nyquist plots, as depicted in Figure 5. Additionally, the data amply demonstrated this improvement with the high fatty inhibitor content.

According to this principle, the excessive passivity action of the metallic surface is the source of the interface's excess electrochemical impedance values in the low frequency zone. Here, the carbon steel's passivation performance is a result of the non-ionic adsorption particles acting in success on polymeric inhibitor against acid's harsh effects [32]. Nonetheless, it is also well known that the bulk size and active centers of corrosion inhibitors play a major role in their effectiveness [33]. As a result, the extra two methylene groups in composite IIb's structure may be the reason for its higher inhibition of corrosion than composite Ib. NH2 has a higher electron-releasing (nucleophilic) character than an electron-withdrawing (electrophonic) character. As a result, Ib and IIb can react with the acid solution to form protonated components in the acidic medium[34]. According to findings from other studies [35–37], this ammonium species may reduce the electronic density on the fatty-based inhibitor composites.

Figure 6 (a, b, c, and b) displays multi-characteristic parts for carbon steel/Ib and IIb compounds/1.0 M HCl system. EIS diagrams were also observed. When the frequency increases in the highest zone, the phase angle values drastically decrease to 0° and the log |Z| values approach 0.5. This appearance results from a method of withstanding and relates to the acidic medium's resistance. A longitudinal relationship between log |Z| and log f, with a slope close to 1, and a phase angle drop of -45°, can be clearly shown in the midstzone of the frequency graph [38, 39]. This look is characteristic of a capacitive way.

A normal capacitive action would have a slope of about 1 and an angle of about -40°; nevertheless,

electrochemical processes frequently behave less than optimally. The electrode's resistive performance increases in the lowest frequency loop zone, but the zone where log |Z| does not depend on log f is not entirely extended.
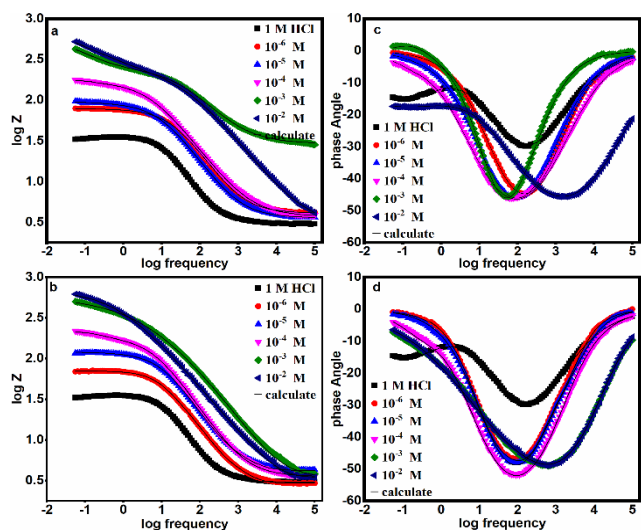
Figure 6 Bode and phase angle plots of the EIS data for carbon steel in 1.0 M HCl in absence and presence of different concentrations of (a and c) Ib and (b and d) IIb compounds.
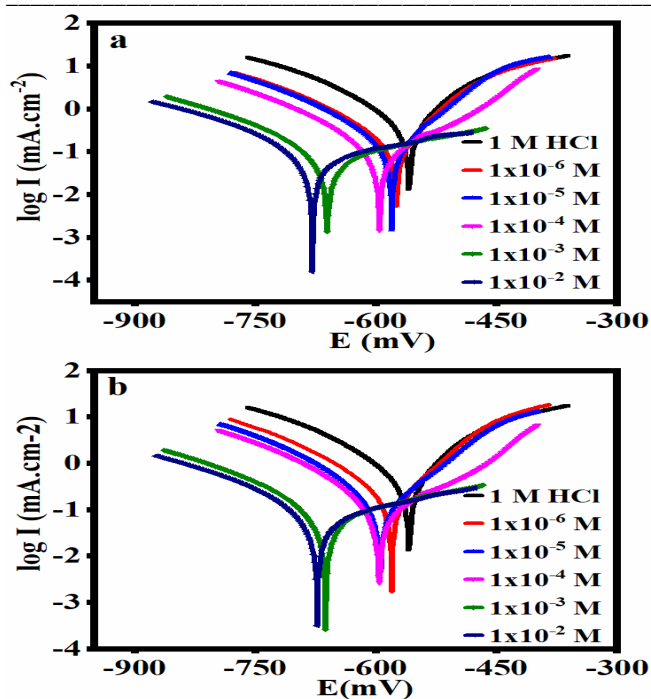
3.5. Potentiodynamic Polarization

PDP technique were operated in the designed acidic solution with and without of the prepared non-ionic polymeric composites. The major electrochemical parameters like corrosion potential (E_{Corr}), corrosion current density (I_{Corr}), corrosion rate (CR), efficiency of corrosion current density (EF_{Icorr}%) and efficiency of corrosion rate (EF_{CR}%) are presented in Table 5.

Table 5: The Polarization parameters for different concentrations of C10 and C12 compounds at ambient temperature in 1 M HCl

Compounds	Parameter Conc. (M)	E_{corr} mV	i_{corr} mA.cm^{-2}	β_a mV	β_c mV	CR mm/Y	R_p ohm.cm²	θ	EF%
	1 M HCl	-558	1.53	166	-198	18	46		
C10	10^{-6}	-575	0.34	94	-149	3.98	117	0.78	78
	10^{-5}	-580	0.30	93	-143	3.45	136	0.80	80
	10^{-4}	-596	0.20	121	-143	2.31	237	0.87	87
	10^{-3}	-660	0.16	586	-184	1.83	410	0.90	90
	10^{-2}	-679	0.13	599	-186	1.52	416	0.92	92
C12	10^{-6}	-580	0.31	91	-129	3.65	102	0.80	80
	10^{-5}	-594	0.29	108	-137	3.38	151	0.81	81
	10^{-4}	-596	0.16	124	-122	1.92	230	0.90	90
	10^{-3}	-663	0.13	504	-167	1.5	406	0.92	92
	10^{-2}	-673	0.12	570	-186	1.45	447	0.93	93

The intensity–potential relationship after exposure the steel electrode to HCl solution with and without definite ratios of inhibitors is exposed in Figure 7. Based on the blank electrolyte without the influence of inhibitor, the carbon steel electrode shows a significant performance.

The passive region of about 200 mV is detected on the anodic site of the polarization graph owing to the formulation of oxide film on the metal superficies. At the border of this stage, the current value increases spectacularly throughout the potential range, correlating the onset of steel decay. According to the backward turn, a hysteresis loop is obtained appearing the presence of digging steel attack.

Figure 7 Potentiodynamic polarization plots for the carbon steel in 1.0 M HCl in absence and presence of different concentrations of (a) Ib and (b) IIb compounds.

By the addition of inhibitor, no significant influence obtained in the cathodic site of the PDP graph. However, the passive zone is clearly increased exhibiting the inhibiting manner of non-ionic polymeric components on the carbon steel in the anodic place. Otherwise, the Potentiodynamic polarization graphs acquired under effect of inhibitor proceed the conformable performance as the passive zone increases and the digging potential gets about fewer negative values with raising the concentration of inhibitor [40,41].

The corrosion potential (E_{corr}) exhibits a light variation with the presence of inhibitor, whilst the corrosion current density (i_{corr}) considerable gets about fewer negative magnitudes. The obtained manner due to branched polymeric constituents with the outer active sites got to be adsorbed on the steel surface by supplants the offensive chlorine ions of the acidic solution. The adsorptive action of inhibitor components from steel was distinguished to its adsorption rate and the corrosion rate raise with increasing potential value. With the excess of inhibitor content, the entire active functional groups-based polymer will be adsorbed until a sufficient film was covered and deposited on the iron electrodes [42].

The values of Tafel cathodic and anodic slopes (bc, ba) were slightly changed in solutions at low concentrations It means that there is no change in the mechanism of cathodic and anodic reaction in the presence of the inhibitor. but at high concentration the value of Tafel anodic slope was highly change that indicate the type of corrosion inhibitor type tended to anodic type. The highest impact of L-cysteine based inhibitor that ensured the steel extended to realize 92% at inhibitor content of 0.01 M. These records are reasonable that the polymeric inhibitor molecules able to clanged on steel to prohibit the

active sites effectively and get a defensive film versus the aggressive attack of acid environment[34].

On the other hand, the obtained results may due to the presence of both (COO) group and (NH₂) group on L-cysteine structure which can easily produce protonated species in HCl medium. This ammonium alternative may decrease the electronic capacity on L-cysteine based composites. Further, based on some literatures, at high inhibitor content, the anionic species exist in the acidic environment can play as effective inhibitors throughout impeding the pores of a passive film produced by the inhibitor's components. In this stage, it will be more complicated for the high protonated fatty inhibitor molecules to switch to the positively charged surface of iron owing to strong electrostatic repulsion force. The anionic molecules are primarily clanged on the metallets the inhibitor constituents to readily come near to the surface [43].

3.6. Surface morphology

SEM is employed to investigate the alterations in morphological structure of the corroded carbon steel surface before and after introducing of L-cysteine based inhibiting composites (Figure 8). Checking of morphological changes of the unprotected carbon steel coupons (Figure 8a) appeared that the carbon steel superficies is extremely deteriorated and corroded. This behaviour proposes that the pure steel surface is substantially damaged as a result of the direct attack of free strong acid medium [44].
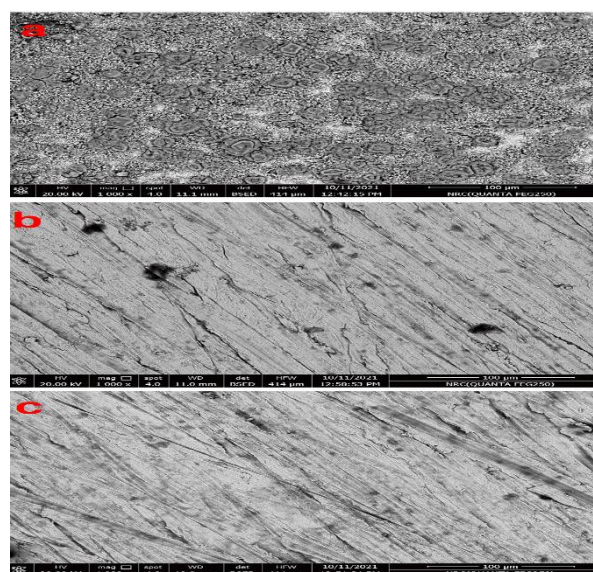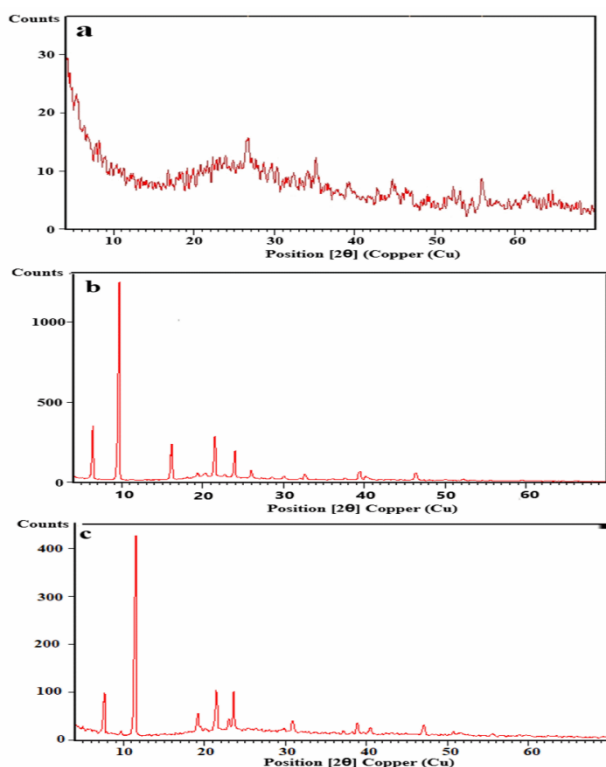

Figure 8 Scanning electron micrographs of the steel surface after 24h immersed in (a) 1.0 M HCl and with 250 ppm of (a) blank (b) Ib and (c) IIb compounds.

Under the influence of 0.01 M of Ib (Figure 8b) and IIb (Figure 8c), SEM images of the inhibited steel surface exposed as linear smooth surface. This significant conception elucidated that the attack is uncommonly decreased with the boost of fatty based inhibitors. The current behaviour is probably owing to the adsorbed inhibitor components on the steel superficies as a preventative film [44].

3.7. X-ray diffraction (XRD) analysis

XRD is utilized to characterize the oxide film founded on the surface with and without the inhibition systems [45]. Spectra of XRD patterns were detected for the pure carbon steel specimens and also for the adsorbed inhibitor-based steel ones by plunging in 1 M HCl medium for 24hrs. In case of unprotected metal, XRD spectra refer clearly to strong attack of metal coupons in the acid which in turns giving rise to the formulation of several magnetite vibrations of iron oxides, appearing at $2\Theta = 27°$, $35°$ and $56°$ as shown in Figure 9a. Otherwise, the recorded XRD data of steel plunged in the designed 1 M HCl medium containing 250 ppm of inhibitor Ib and IIb are shown in Figures 9b and 9c, respectively. For both systems, the vibration intensity peak of iron exposes mainly appeared at $2\Theta = 9.5$ and $2\Theta = 11.2$, respectively. It is reveals that the vibration patterns owing to the presence of iron oxides are not found. This significant alteration in spectral records of steel proposes the formation of chelation between iron and inhibitor on the steel. The small difference between XRD spectra of systems Ib and IIb may related to the chain length of the fatty acid-based inhibitor. These given outcomes confirm the prospect of other preservative film formation based on heteroatoms like nitrogen, oxygen and sulphur exist in the inhibitor structure as well [46].
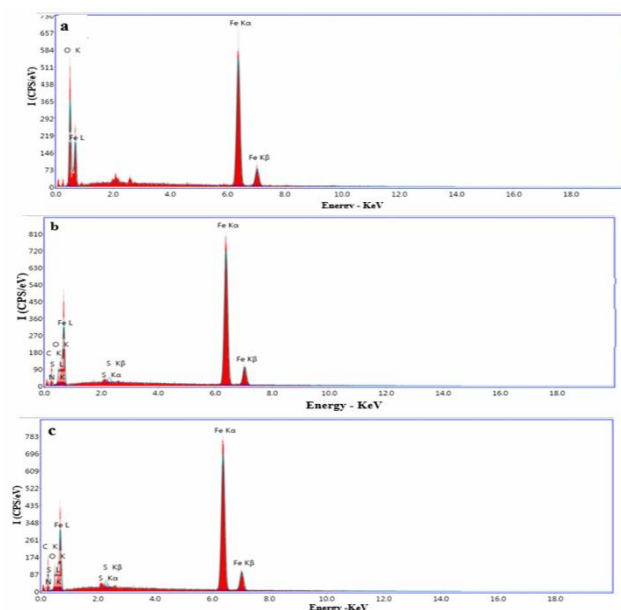
Figure 9 *X-ray diffraction of the steel surface after 24h immersed in (a) 1.0 M HCl and with 250 ppm of (a) blank (b) Ib and (c) IIb compounds.*

3.8. Energy dispersive X-ray (EDX) analysis

EDAX (Figure 10) is employed to identify the elemental analysis for film formation on metal from holding the inhibitor fragments in the acid media. It is reveals that the presence of Ib and IIb inhibitors (Figures 10b and 10c) leads to the formation of the distinctive peak of carbon, oxygen, nitrogen and sulfur, that are present in the chemical structure of the prepared inhibitor systems. Moreover, the common iron peaks are considerably repressed comparative to unprotected carbon steel surface specimens (Figures10a).

Figure 10 *Energy dispersive X-ray analysis of the steel surface after 24h immersed in (a) 1.0 M HCl and with 250 ppm of (a) blank (b) Ib and (c) IIb compounds*

All such iron spectra lines formed owing to the accumulation on the metal [45]. Additionally, EDAX analysis records the percentage (wt%) of elements exist on steel surface in 1 M HCl solution prior and in accordance of inhibitors as illustrated in Table6.

Table 6: The elemental analysis for film formation on the carbon steel surface from adsorption the inhibitor compounds in the acid media

Elements Compounds	O	N	S	C	Fe
1 M HCl	20	-	-	-	80
C10	5	1.2	0.79	14	79
C12	4	0.82	1.04	18	74

The data analysis of EDAX measurements of carbon steel in the two cases exhibited that the carbon steel surface was clearly deteriorated in the strong medium and had high C content of 14% and 18%, moderate O content 5% and 4%, low content of S and N for Ib and IIb inhibitors, respectively. These records emphasize the production of a shielding film by inhibitor components. Extremely little contents of S and N on the metal face with the addition of inhibitor may owe to the production of attack species [46,47].

4. CONCLUSIONS

Corrosion suppression, electrochemical and adsorptive properties of modern non-ionic polymeric surfactants containing fatty acids, polyethylene glycol and L-cysteine compounds are studied. Decanoate and dodecanoate-PEG 600 were reacted to form long chain ester structures. Moreover, L-cysteine component was joined to the structure with branched thiol linkage. The

designed non-ionic polymeric surfactants, capriate L-cysteinate polyethylene glycol (Ib) and laurate L-cysteinate polyethylene glycol (IIb), having both hydrophilic–hydrophobic nature. The obtained Ib and IIb systems were characterized throughout the standard electrochemical techniques such as FT-IR, XRD and EDAX. Surface active characterization and thermodynamic performance based on the concentration of the elaborated compounds were discussed. The adsorption pathway was detected convenient through the Langmuir adsorption isotherm. Polarization patterns exposed that the prepared fatty compounds were mixed–type corrosion inhibitors. The results reveal that these fatty-L-cysteine compounds have a significant corrosion inhibition and their protection performance as the order: IIb > Ib. Morphological structure of carbon steel prior and in accordance of the inhibitor in the acid medium was tested. The uncovered steel samples shown that the surface is corroded and damaged, meanwhile with Ib and IIb systems, the surface appeared smooth. XRD exposes high attack of steel acid medium while with inhibitor the formation of iron oxides exists. With Ib and IIb systems, EDAX peaks of C, O, N and S contains inhibitor structure are observed. Fe peaks are repressed compared with uncovered steel. These significant spectra may due to the overlying on metal surface.

CONFLICTS OF INTEREST

The authors declare that they have no known competing financial interests or personal relationships that could have appeared to influence the work reported in this paper.

REFERENCES

[1] A.A. Siyal, M.R. Shamsuddin, A. Low, Fly ash based geopolymer for the adsorption of cationic and nonionic surfactants from aqueous solution–A feasibility study, Mater. Lett. 283 (2021) 128758.

[2] H. Cortés, H. Hernández-Parra, S.A. Bernal-Chávez, M.L. Del Prado-Audelo, I.H. Caballero-Florán, F. V Borbolla-Jiménez, M. González-Torres, J.J. Magaña, G. Leyva-Gómez, Non-ionic surfactants for stabilization of polymeric nanoparticles for biomedical uses, Materials (Basel). 14 (2021) 3197.

[3] R. Gamal, S.E. Rizk, N.E. El-Hefny, The adsorptive removal of Mo (VI) from aqueous solution by a synthetic magnetic chromium ferrite nanocomposite using a nonionic surfactant, J. Alloys Compd. 853 (2021) 157039.

[4] G. Zhang, Y. Chen, X. Sui, M. Kang, Y. Feng, H. Yin, Nonionic surfactant stabilized polytetrafluoroethylene dispersion: Effect of molecular structure and topology, J. Mol. Liq. 345 (2022) 116988.

[5] A. El Monem Eissa, M. El Hefnawy, M.D. Allah, Synthesis and evaluation of nonionic polymeric surfactants based on acrylated polyethylene glycol, J. Surfactants Deterg. 16 (2013) 161–171.

[6] Y. He, K. Xu, X. Feng, L. Chen, Z. Jiang, A nonionic polymer-brush-grafted PVDF membrane to analyse fouling during the filtration of oil/water emulsions, J. Memb. Sci. 637 (2021) 119644.

[7] A.S. Ismail, Nano-sized aluminum coatings from aryl-substituted imidazolium cation based ionic liquid, Egypt. J. Pet. 25 (2016) 525–530.

[8] A.S. Ismail, Electrodeposition of aluminium–copper alloy from 1-butyl-1-methylpyrrolidinium bis (trifluoromethylsulfonyl) imide ionic liquid, Egypt. J. Pet. 26 (2017) 61–65.

[9] X. Cheng, J. Xia, R. Wu, W. Jin, C. Pan, Optimisation of sacrificial anode cathodic protection system in chloride-contaminated reinforced concrete structure, J. Build. Eng. 45 (2022) 103515.

[10] M. Nagels, B. Verhoeven, N. Larché, R. Dewil, B. Rossi, Corrosion behaviour of lean duplex stainless steel in advanced oxidation process (AOP) based wastewater treatment plants, Eng. Fail. Anal. 136 (2022) 106170.

[11] M.A. Abbas, E.I. Arafa, E.S. Gad, M.A. Bedair, O.E. El-Azabawy, H.I. Al-Shafey, Performance Assessment by Experimental and Theoretical Approaches of Newly Synthetized Benzyl Amide Derivatives as Corrosion Inhibitors for Carbon Steel in 1.0 M Hydrochloric Acid Environment, Inorg. Chem. Commun. (2022) 109758.

[12] M.A. Abbas, A.M. Eid, M.M. Abdou, A. Elgendy, R.A. El-Saeed, E.G. Zaki, Multifunctional Aspects of the Synthesized Pyrazoline Derivatives for AP1 5L X60 Steel Protection Against MIC and Acidization: Electrochemical, In Silico, and SRB Insights, ACS Omega. 6 (2021) 8894–8907.

[13] M.A. Abbas, K. Zakaria, A.M. El-Shamy, S.Z. El Abedin, Utilization of 1-butylpyrrolidinium chloride ionic liquid as an eco-friendly corrosion inhibitor and biocide for oilfield equipment: combined weight loss, electrochemical and SEM studies, Zeitschrift Für Phys. Chemie. 235 (2021) 377–406.

[14] K. Abderrahim, O.M.A. Khamaysa, I. Selatnia, H. Zeghache, Adsorption and performance assessment of 5-Mercapto-1-Methyl Tetrazole as A9M steel corrosion inhibitor in HCl medium: A detailed experimental, and computational methods., Chem. Data Collect. 39 (2022) 100848.

[15] C. Verma, C.M. Hussain, M.A. Quraishi, A. Alfantazi, Green surfactants for corrosion control: Design, performance and applications, Adv. Colloid Interface Sci. 311 (2023) 102822.

[16] A.A. Farag, A.S. Ismail, M.A. Migahed, Environmental-friendly shrimp waste protein corrosion inhibitor for carbon steel in 1 M HCl solution, Egypt. J. Pet. 27 (2018) 1187–1194.

[17] C. Gong, T. Zhao, Y. Zhao, G. Zhang, Effects of oxyethylene groups on the adsorption behavior and application performance of long alkyl chain phosphate surfactants, J. Mol. Liq. 345 (2022) 117044.

[18] C. Verma, M.A. Quraishi, K.Y. Rhee,

Hydrophilicity and hydrophobicity consideration of organic surfactant compounds: Effect of alkyl chain length on corrosion protection, Adv. Colloid Interface Sci. 306 (2022) 102723.

[19] M. Mobin, S. Zehra, M. Parveen, L-Cysteine as corrosion inhibitor for mild steel in 1 M HCl and synergistic effect of anionic, cationic and non-ionic surfactants, J. Mol. Liq. 216 (2016) 598–607.

[20] A.A. Farag, A.S. Ismail, M.A. Migahed, Squid by-product gelatin polymer as an eco-friendly corrosion inhibitor for carbon steel in 0.5 M H2SO4 solution: experimental, theoretical, and Monte Carlo simulation studies, J. Bio-and Tribo-Corrosion. 6 (2020) 1–15.

[21] S.O. Badmus, H.K. Amusa, T.A. Oyehan, T.A. Saleh, Environmental risks and toxicity of surfactants: overview of analysis, assessment, and remediation techniques, Environ. Sci. Pollut. Res. 28 (2021) 62085–62104.

[22] P.A. Cornwell, A review of shampoo surfactant technology: consumer benefits, raw materials and recent developments, Int. J. Cosmet. Sci. 40 (2018) 16–30.

[23] A.I. Adawy, R.M. Soliman, A.S. Dhmees, Z.I. Abdeen, Antimicrobial activity of polymeric surfactants blending with zinc oxide nanoparticles derived from Electric Arc Furnace Dust, Egypt. J. Chem. 64 (2021) 2–3.

[24] M.J. Rosen, J.T. Kunjappu, Surfactants and interfacial phenomena, John Wiley & Sons, 2012.

[25] S.M. Shaban, S. Abd Elsamad, S.M. Tawfik, A.-H. Adel, I. Aiad, Studying surface and thermodynamic behavior of a new multi-hydroxyl Gemini cationic surfactant and investigating their performance as corrosion inhibitor and biocide, J. Mol. Liq. 316 (2020) 113881.

[26] R.-Y. Hong, J.-H. Li, S.-Z. Zhang, H.-Z. Li, Y. Zheng, J. Ding, D.-G. Wei, Preparation and characterization of silica-coated Fe3O4 nanoparticles used as precursor of ferrofluids, Appl. Surf. Sci. 255 (2009) 3485–3492.

[27] I.M. Kooter, A.J. Pierik, M. Merkx, B.A. Averill, N. Moguilevsky, A. Bollen, R. Wever, Difference Fourier transform infrared evidence for ester bonds linking the heme group in myeloperoxidase, lactoperoxidase, and eosinophil peroxidase, J. Am. Chem. Soc. 119 (1997) 11542–11543.

[28] A.I. Adawy, M.A. Abbas, K. Zakaria, New Schiff base cationic surfactants as corrosion inhibitors for carbon steel in acidic medium: weight loss, electrochemical and SEM characterization techniques, Res. Chem. Intermed. 42 (2016) 3385–3411.

[29] I. Aiad, M.A. Riya, S.M. Tawfik, M.A. Abousehly, Synthesis, surface properties and biological activity of N, N, N-tris (hydroxymethyl)-2-oxo-2-(2-(2-(alkanoyloxy) ethoxy) ethoxy) ethanaminium chloride surfactants, Egypt. J. Pet. 25 (2016) 299–307.

[30] L.B. Coelho, M. Lukaczynska-Anderson, S. Clerick, G. Buytaert, S. Lievens, H.A. Terryn, Corrosion inhibition of AA6060 by silicate and phosphate in automotive organic additive technology coolants, Corros. Sci. 199 (2022) 110188.

[31] H. Kumar, H. Raj, S. Sharma, H. Dahiya, Corrosion inhibition and adsorption studies of Ammonium oxalate for mild steel by computational and experimental techniques: A sustainable approach, Chem. Data Collect. 36 (2021) 100785.

[32] M.A. Sobhy, M. Abbas, A.A. El-Zomrawy, Evaluation of Aloe vera Gel extract as eco-friendly corrosion inhibitor for carbon steel in 1.0 M HCl, Egypt. J. Chem. 64 (2021) 5–6.

[33] M.A. Abbas, A.S. Ismail, K. Zakaria, A.M. El-Shamy, S.Z. El Abedin, Adsorption, thermodynamic, and quantum chemical investigations of an ionic liquid that inhibits corrosion of carbon steel in chloride solutions, Sci. Rep. 12 (2022) 12536.

[34] C. Verma, M.A. Quraishi, C.M. Hussain, Greenly synthesized zeolites as sustainable materials for corrosion protection: Design, technology and application, Adv. Colloid Interface Sci. (2023) 102868.

[35] D.K. Verma, F. Khan, Corrosion inhibition of mild steel in hydrochloric acid using extract of glycine max leaves, Res. Chem. Intermed. 42 (2016) 3489–3506.

[36] T. Zheng, J. Liu, M. Wang, Q. Liu, J. Wang, Y. Chong, G. Jia, Synergistic corrosion inhibition effects of quaternary ammonium salt cationic surfactants and thiourea on Q235 steel in sulfuric acid: Experimental and theoretical research, Corros. Sci. 199 (2022) 110199.

[37] A.O. Alnajjar, H.M. Abd El-Lateef, A novel approach to investigate the synergistic inhibition effect of nickel phosphate nanoparticles with quaternary ammonium surfactant on the Q235-mild steel corrosion: surface morphology, electrochemical-computational modeling outlines, J. Mol. Liq. 337 (2021) 116125.

[38] C. Verma, A. Alfantazi, M.A. Quraishi, K.Y. Rhee, Significance of Hammett and Taft substituent constants on bonding potential of organic corrosion inhibitors: Tailoring of reactivity and performance, Coord. Chem. Rev. 495 (2023) 215385.

[39] C. Verma, L.K.M.O. Goni, I.Y. Yaagoob, H. Vashisht, M.A.J. Mazumder, A. Alfantazi, Polymeric surfactants as ideal substitutes for sustainable corrosion protection: A perspective on colloidal and interface properties, Adv. Colloid Interface Sci. (2023) 102966.

[40] C.A. Loto, O.S.I. Fayomi, R.T. Loto, A.P.I. Popoola, Potentiodynamic Polarization and Gravimetric Evaluation of Corrosion of Copper in 2M H2SO4 and its inhibition with Ammonium Dichromate, Procedia Manuf. 35 (2019) 413–418.

[41] A.I. Adawy, M.A. Abbas, K. Zakaria, Synthesis, surface properties, and biological activity of some cationic surfactant complexes, Mol. Cryst. Liq. Cryst. 724 (2021) 77–89.

[42] M. Ouakki, M. Galai, Z. Benzekri, Z. Aribou, E. Ech-chihbi, L. Guo, K. Dahmani, K. Nouneh, S. Briche, S. Boukhris, A detailed investigation on the corrosion inhibition effect of by newly synthesized pyran derivative on mild steel in 1.0 M HCl: Experimental, surface morphological (SEM-EDS, DRX& AFM) and computational analysis (DFT & MD simulation), J. Mol. Liq. 344 (2021) 117777.

[43] S. Boukazoula, D. Haffar, R. Bourzami, L. Toukal, V. Dorcet, Synthesis, characterizations, crystal structure, inhibition effects and theoretical study of novel Schiff base on the corrosion of carbon steel in 1 M HCl, J. Mol. Struct. 1261 (2022) 132852.

[44] B.X. Vuong, T.L. Huynh, T.Q.N. Tran, S.V.P. Vattikuti, T.D. Manh, P. Nguyen-Tri, A.T. Nguyen, P. Van Hien, N.N. Dang, Corrosion inhibition of carbon steel in hydrochloric acid solution by self-formation of a Malpighia glabra leaf extract-based organic film, Mater. Today Commun. 31 (2022) 103641.

[45] F.U. Ermawati, XRD and EDX Analyses on the Formation of MgTiO3 Phase in (Mg0. 6Zn0. 4)(Ti0. 99Sn0. 01) O3 Powders Due to Calcination Temperature Variations, in: J. Phys. Conf. Ser., IOP Publishing, 2021: p. 12009.

[46] M.A. Abbas, E.I. Arafa, M.A. Bedair, A.S. Ismail, O.E. El-Azabawy, S.A. Baker, H.I. Al-Shafey, Synthesis, Characterization, Thermodynamic Analysis and Quantum Chemical Approach of Branched N, N′-bis (p-hydroxybenzoyl)-Based Propanediamine and Triethylenetetramine for Carbon Steel Corrosion Inhibition in Hydrochloric Acid Medium, Arab. J. Sci. Eng. 48 (2023) 7463–7484.

[47] H. Kariem, T. Kiefer, C. Hellmich, W. Gaggl, A. Steiger-Thirsfeld, J. Füssl, EDX/XRD-based identification of micrometer-sized domains in scanning electron micrographs of fired clay, Mater. Struct. 53 (2020) 1–20.

Table (1): Surface properties of polymeric surfactants at 40, 50, 60, 70 °C.

Temperature.	Surfactant	$CMC \times 10^{-3}$, Mole/liter	π_{CMC}, mN/m	$Pc_{20} \times 10^{-5}$, Mole/liter	$\Gamma_{max} \times 10^{-11}$, Mole/cm^2	A_{min}, nm^2
40 °C	Ib	3.2	25.3	15	6.1	2.7
	IIb	3	26.3	7.9	6.2	2.6
50 °C	Ib	2.8	26.2	7.9	6.2	2.6
	IIb	2.4	27	4	6.3	2.6
60 °C	Ib	2.2	26.8	4	6.4	2.5
	IIb	2	27.7	2	6.5	2.5
70 °C	Ib	1.8	27.5	2	6.6	2.5
	IIb	1.6	28.1	1.6	6.7	2.5

Table (2): Thermodynamic parameters of micellization of polymeric surfactants at 40, 50, 60, 70 °C.

Temperature	Surfactant	$\Delta G^o_{mis.}$ KJ/mole	$\Delta H^o_{mis.}$ KJ/mole
40 °C	Ib	-14.9	43.1
	IIb	-15.1	-49.5
50 °C	Ib	-15.8	-44.8
	IIb	-16.2	-51.7
60 °C	Ib	-17.0	-50.2
	IIb	-17.2	-53.8
70 °C	Ib	-18.0	-52.3
	IIb	-18.3	-56.1

Table (3): Thermodynamic parameters of adsorption of polymeric surfactants at 40, 50, 60, 70 °C.

Temperature	Surfactant	$\Delta G^o_{ads.}$ KJ/mole	$\Delta H_{ads.}$ KJ/mole
40 °C	Ib	-53.0	-168.9
	IIb	-46.8	-360.0
50 °C	Ib	-56.7	-176.4
	IIb	-56.8	-380.0
60 °C	Ib	-58.9	-185.5
	IIb	-50.6	-440.0
70 °C	Ib	-62.7	-193.0
	IIb	-62.3	-464.0

Table 4: The impedance parameters for different concentrations of C10 and C12 compounds at ambient temperature in 1 M HCl

| Inhibitor compound	Conc. (M)	R_s ohm.cm^2	Q (S Sec^{n}m^{-2}) x10^{-5}	C_f	$N \times 10^{-2}$	R_{ct} ohm.cm^2	Q (S Sec^{n}m^{-2}) x10^{-5}	$n \times 10^{-2}$	R_{ct} ohm.cm^2	C_{dl} μF/cm^2	α°	S	θ	$\%\eta_{Rct}$
	1MHCl	3.1±0.1	-	-	-	-	74±6.1	84±1	32±0.6	362	-30	-0.20		
C10	10^{-6}	4.1±0.1	-	-	-	-	38±0.5	74±0.8	75±9	109	-45	-0.16	0.57	57
	10^{-5}	3.6±0.1	-	-	-	-	38±3	72±0.7	91±1.4	103	-46	-0.09	0.65	65
	10^{-4}	3.7±0.1	-	-	-	-	27±2.5	76±0.6	172±2.9	102	-46	-0.05	0.81	81
	10^{-3}	2.6±0.1	0.16±0.4	23	63±0.4	219±2.5	19±4.3	78±1.3	361±13	89	-46	-0.03	0.91	91
	10^{-2}	3.3±0.3	0.14±1.3	15	62±1	199±2.4	15±0.3	78±0.9	600±17	80	-46	-0.01	0.95	95
C12	10^{-6}	3.2±0.1	-	-	-	-	36±1.7	75±0.17	69±1.5	105	-47	-0.23	0.54	54
	10^{-5}	4.2±0.1	-	-	-	-	32±4	74±1	116±1.4	100	-48	-0.14	0.72	72
	10^{-4}	2.3±0.1	-	-	-	-	28±1.9	71±0.6	218±3.4	89	-49	-0.11	0.85	85
	10^{-3}	2.8±0.1	-	-	-	-	17±1.4	76±0.6	564±11	81	-49	-0.03	0.94	94
	10^{-2}	4.5±0.1	-	-	-	-	13±2	80±0.6	747±19	73	-52	-0.02	0.96	96

Table 5: The Polarization parameters for different concentrations of C10 and C12 compounds at ambient temperature in 1 M HCl

Compounds	Parameter Conc. (M)	E_{corr} mV	i_{corr} mA.cm^{-2}	β_a mV	β_c mV	CR mm/Y	R_p ohm.cm^2	θ	EF%
	1 M HCl	-558	1.53	166	-198	18	46		
C10	10^{-6}	-575	0.34	94	-149	3.98	117	0.78	78
	10^{-5}	-580	0.30	93	-143	3.45	136	0.80	80
	10^{-4}	-596	0.20	121	-143	2.31	237	0.87	87
	10^{-3}	-660	0.16	586	-184	1.83	410	0.90	90
	10^{-2}	-679	0.13	599	-186	1.52	416	0.92	92
C12	10^{-6}	-580	0.31	91	-129	3.65	102	0.80	80

10^{-5}	-594	0.29	108	-137	3.38	151	0.81	81
10^{-4}	-596	0.16	124	-122	1.92	230	0.90	90
10^{-3}	-663	0.13	504	-167	1.5	406	0.92	92
10^{-2}	-673	0.12	570	-186	1.45	447	0.93	93

Table 6: The elemental analysis for film formation on the carbon steel surface from adsorption the inhibitor compounds in the acid media

Elements Compounds	O	N	S	C	Fe
1 M HCl	20	-	-	-	80
C10	5	1.2	0.79	14	79
C12	4	0.82	1.04	18	74
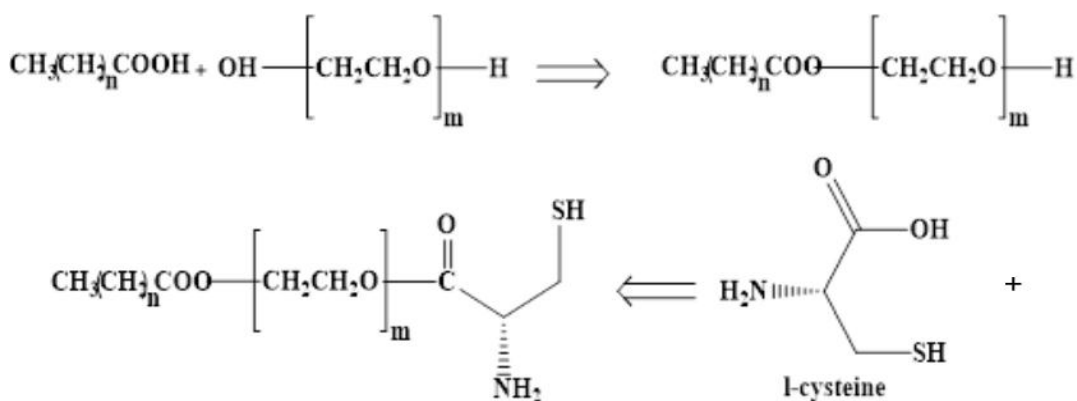
Figure 1 Preparation of Nonionic surfactants based on PEG (M.wt. = 600): n = 8, decanoate -L-cysteinate polyethylene glycol (Ib) and n=10, laurate - L-cysteinate polyethylene glycol (IIb).
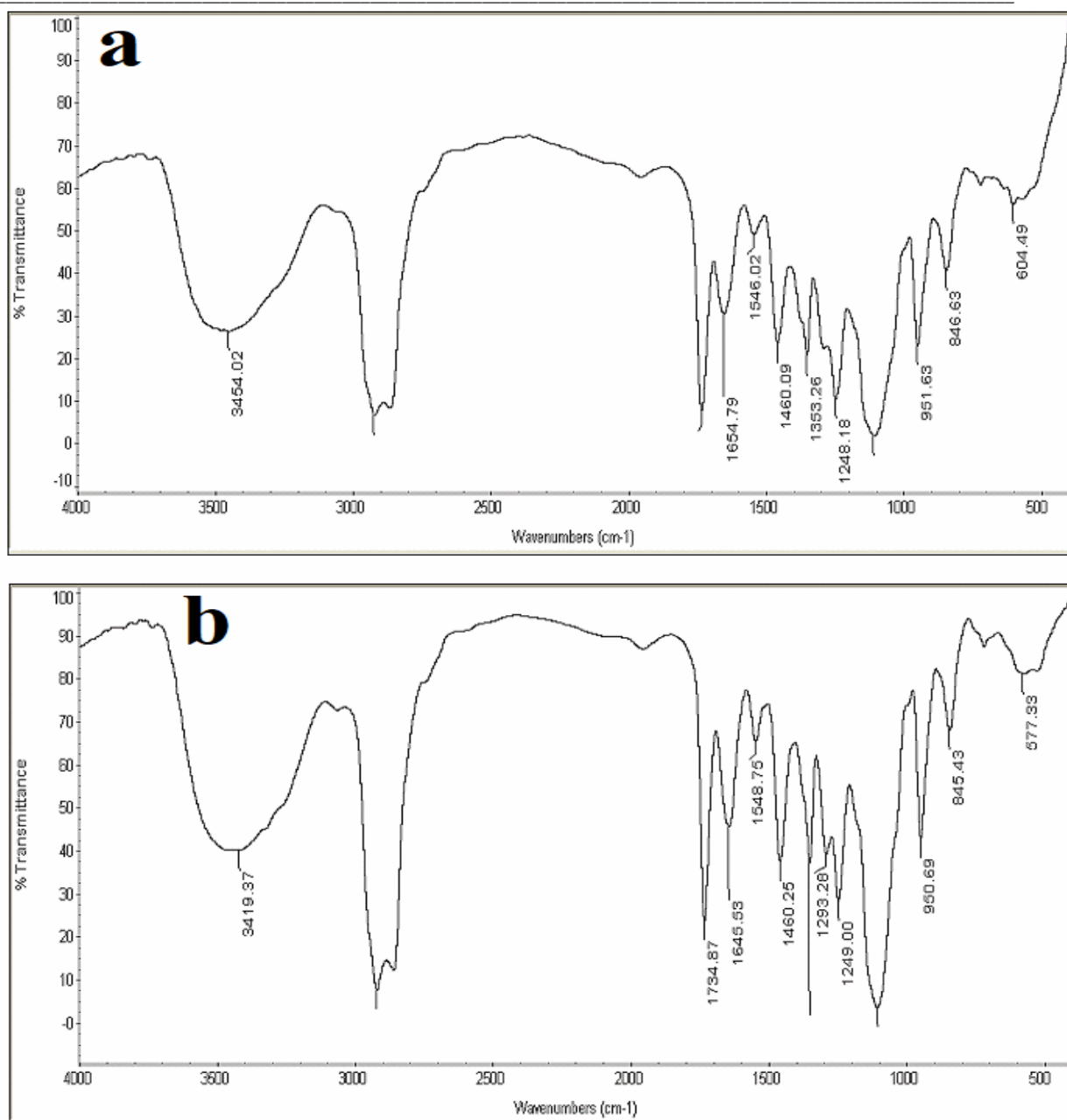
Figure 2 FTIR of Nonionic polymeric surfactant (a) Ib and (b) IIb compounds.
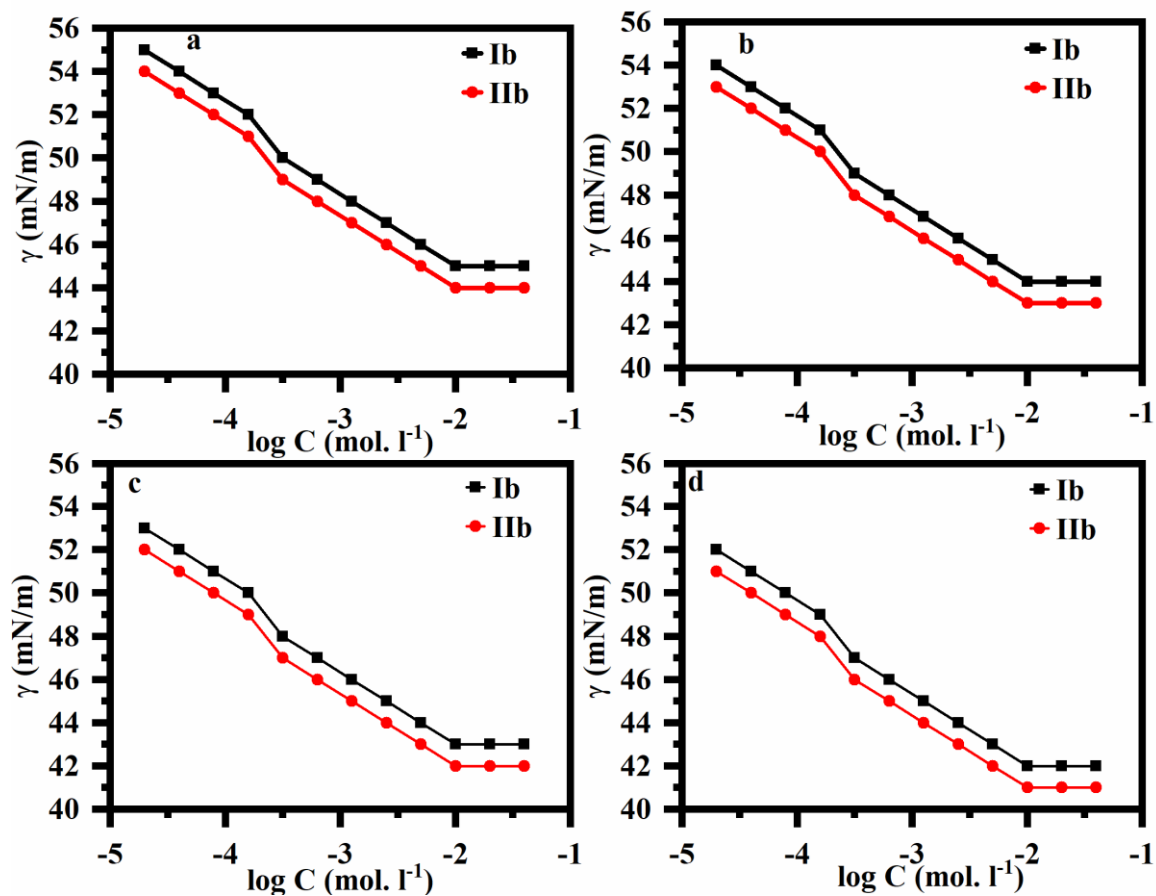
Figure 3 Surface tension vs. log Concentration of synthesized polymeric surfactants (a) Ib and (b) IIb compounds at: (a) 40 ⁰C, (b) 50 ⁰C, (c) 60 ⁰C, (d) 70 ⁰C.
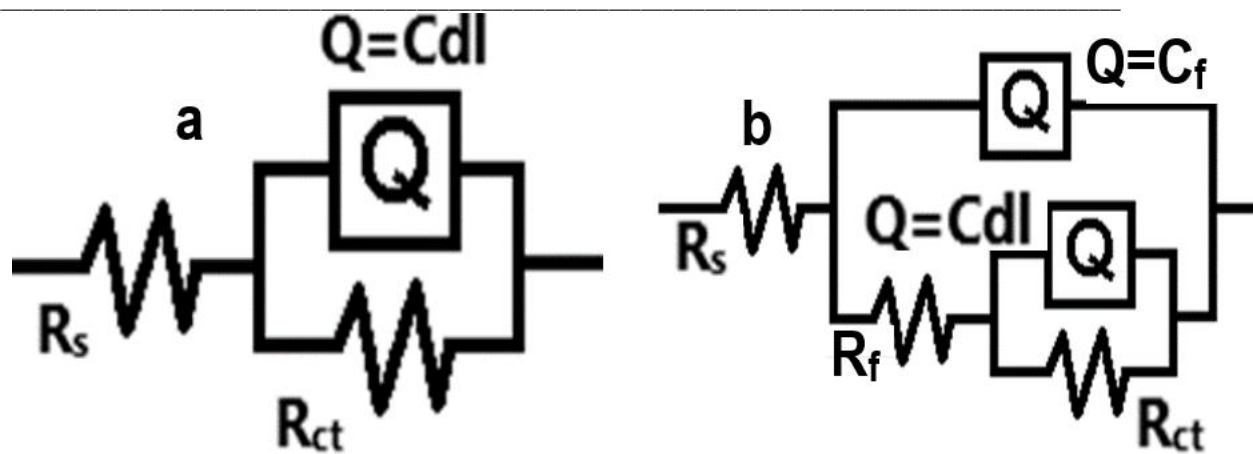
Figure 4 the equivalent circuit model used to fit the EIS data (a) for blank and small concentration (b) for high coccentration.
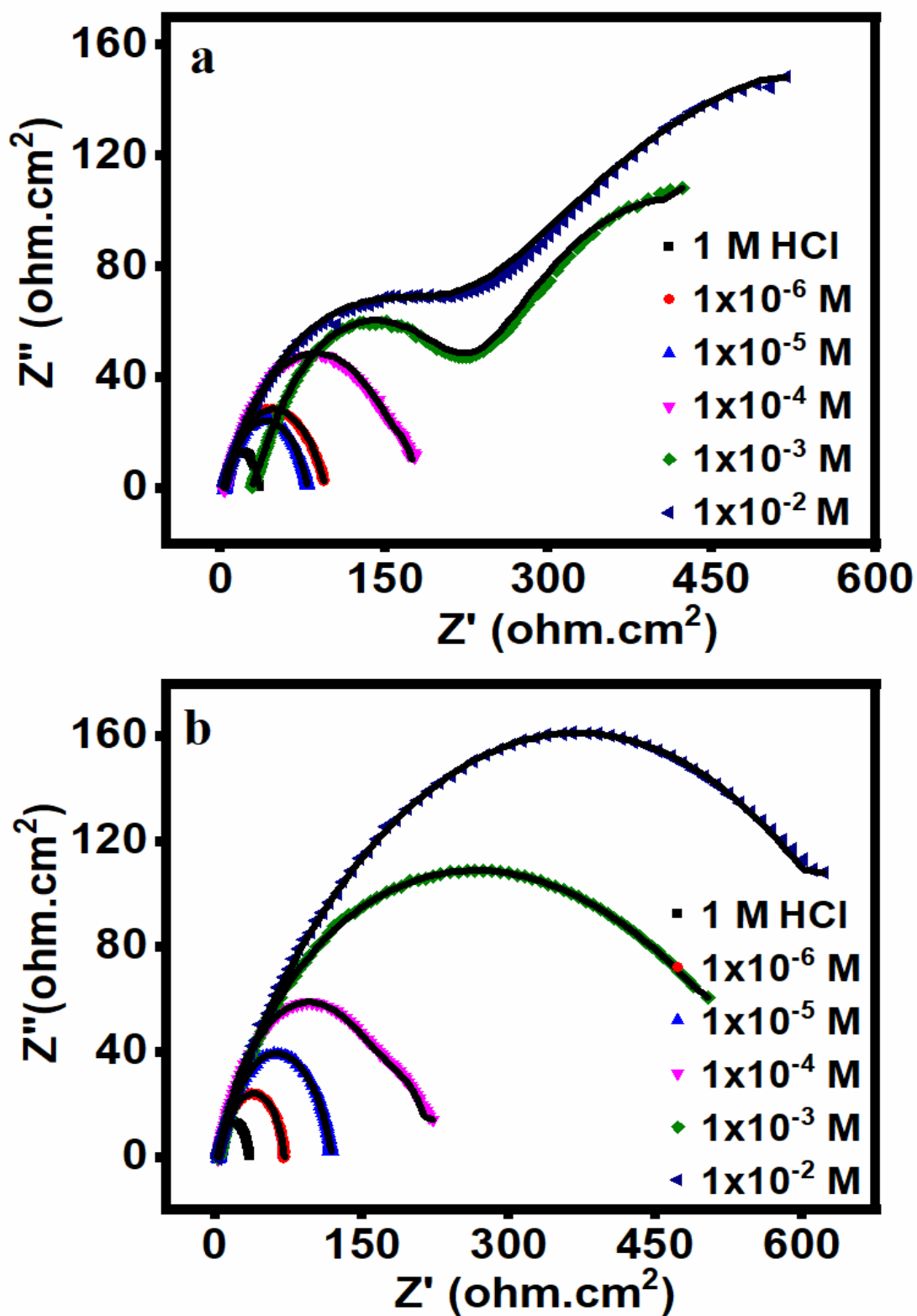
Figure 5 EIS Nyquist plot of the EIS data for carbon steel in 1.0 M HCl in absence and presence of different concentrations of (a) Ib and (b) IIb compounds.
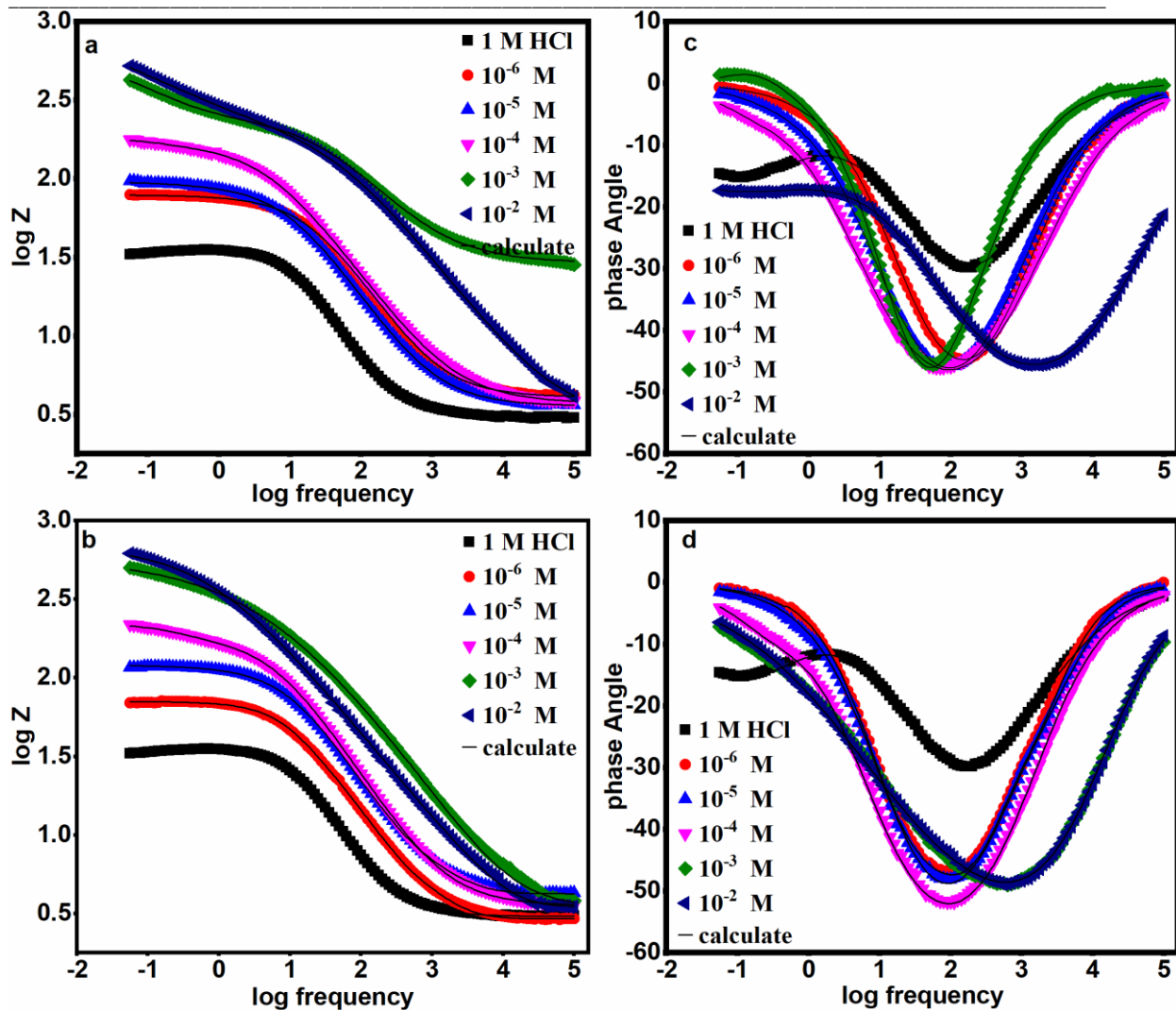
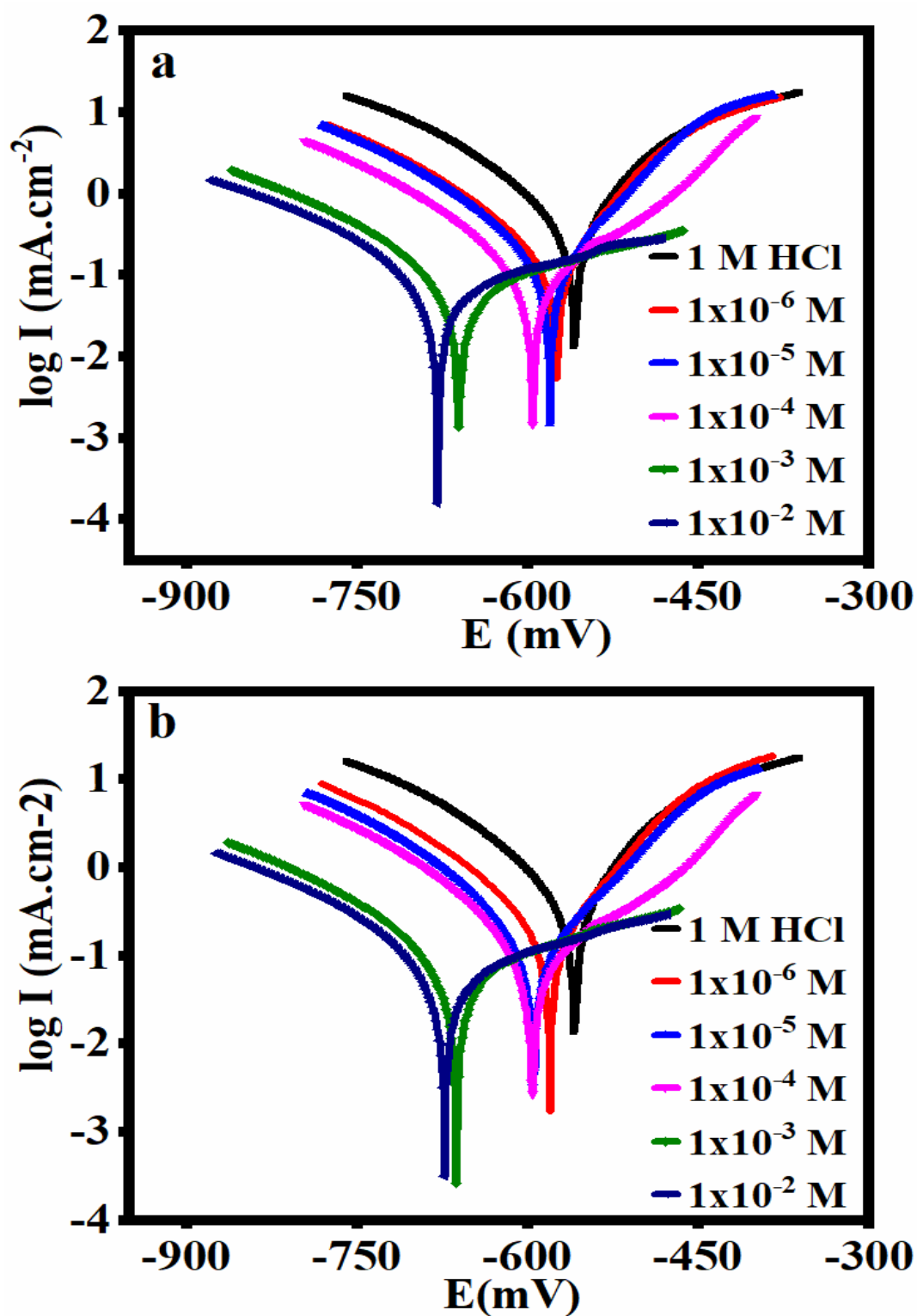**Figure 6** Bode and phase angle plots of the EIS data for carbon steel in 1.0 M HCl in absence and presence of different concentrations of (a and c) Ib and (b and d) IIb compounds.

Figure 7 Potentiodynamic polarization plots for the carbon steel in 1.0 M HCl in absence and presence of different concentrations of (a) Ib and (b) IIb compounds.
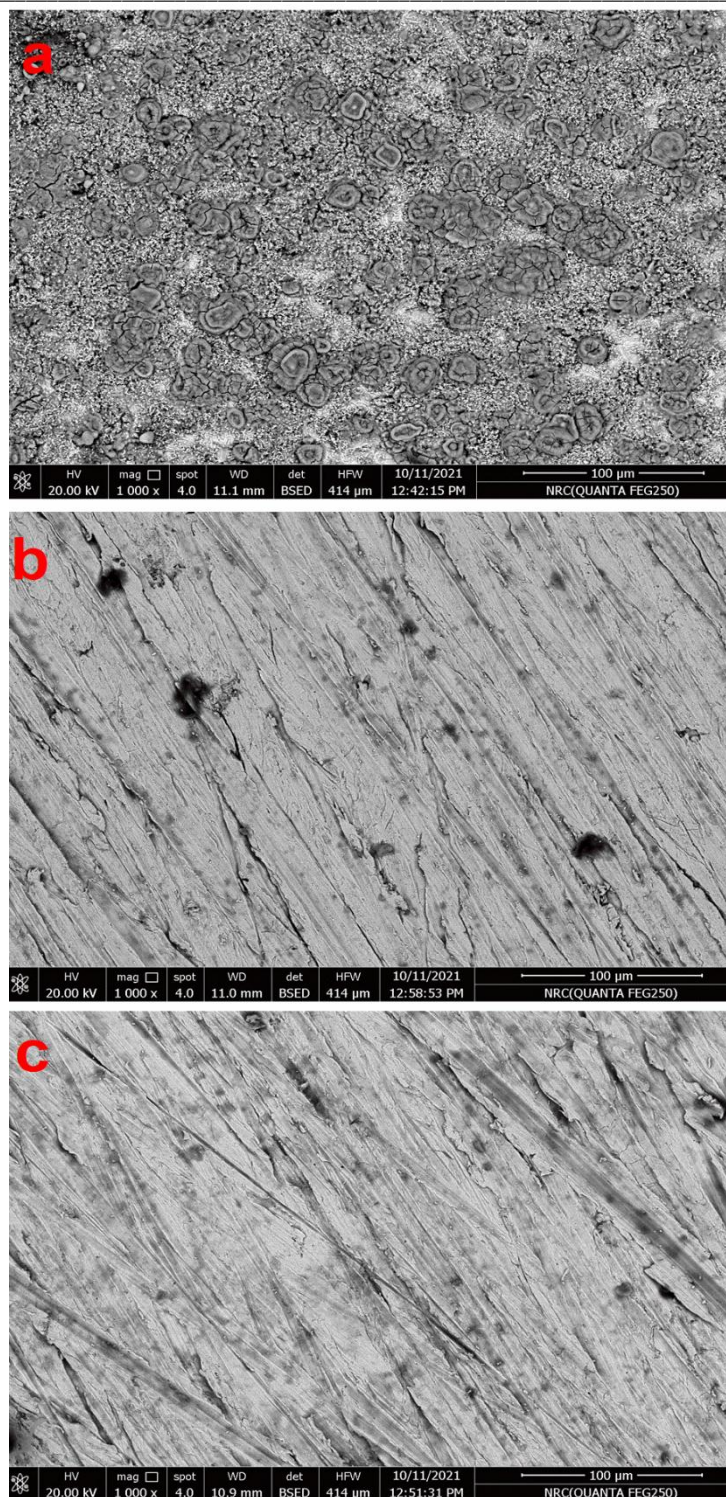
Figure 8 Scanning electron micrographs of the steel surface after 24h immersed in (a) 1.0 M HCl and with 250 ppm of (a) blank (b) Ib and (c) IIb compounds.
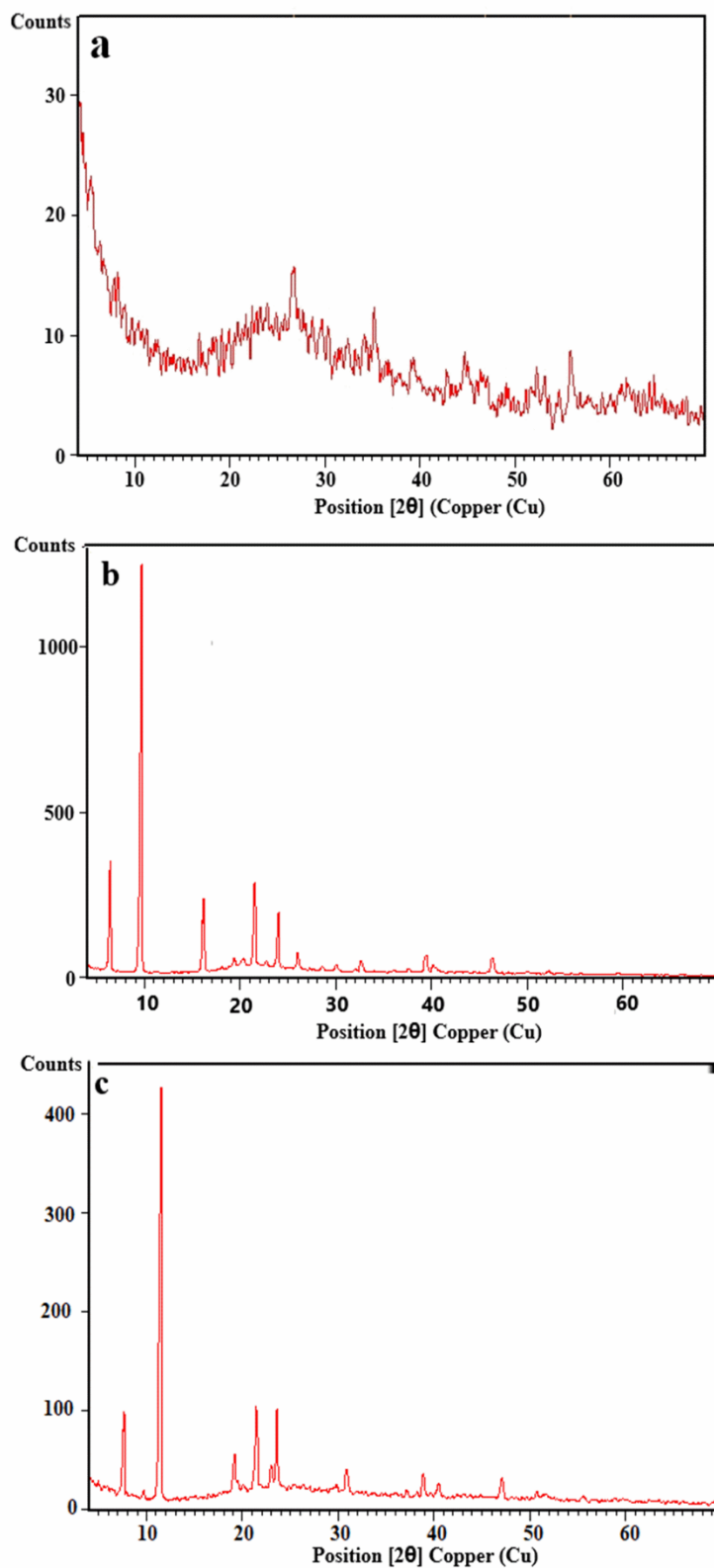
Figure 9 X-ray diffraction of the steel surface after 24h immersed in (a) 1.0 M HCl and with 250 ppm of (a) blank (b) Ib and (c) IIb compounds.
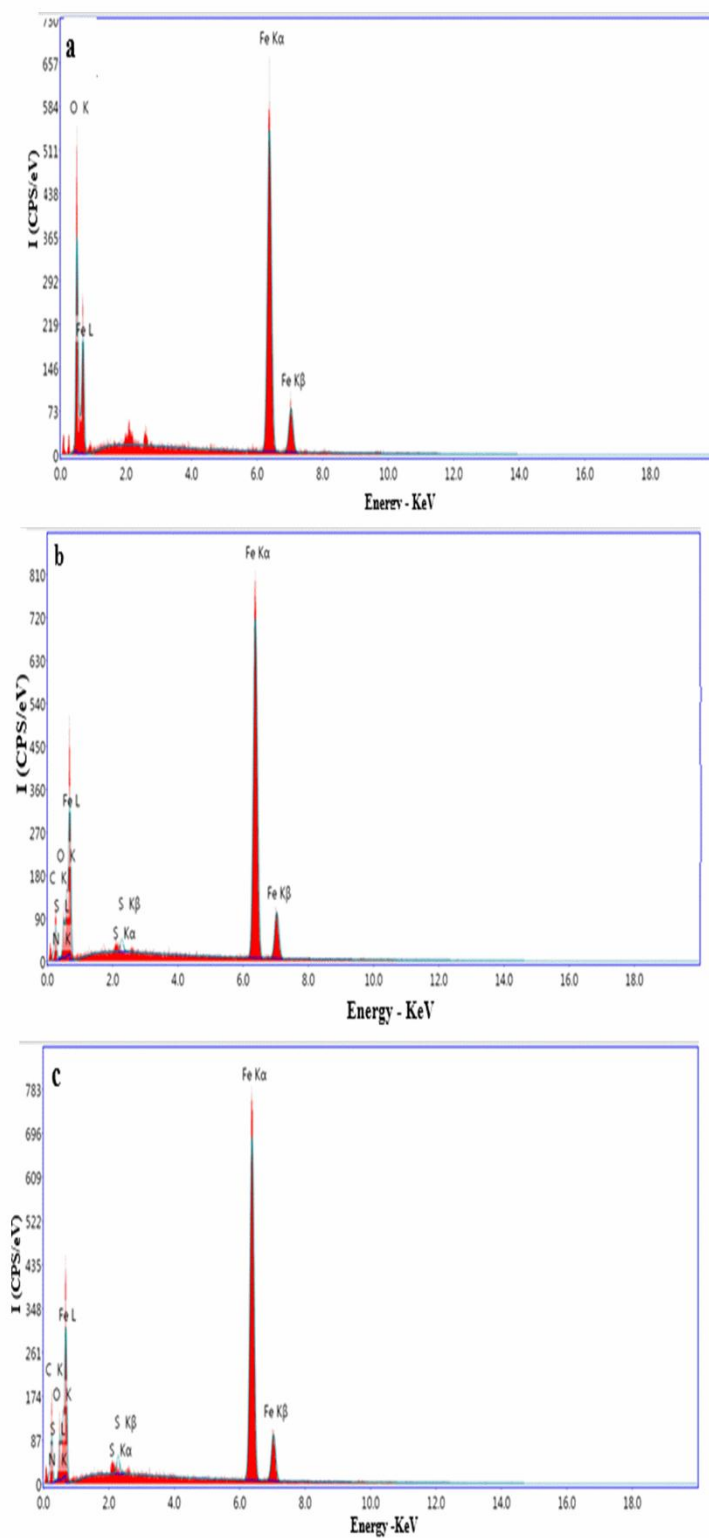
Figure 10 Energy dispersive X-ray analysis of the steel surface after 24h immersed in (a) 1.0 M HCl and with 250 ppm of (a) blank (b) Ib and (c) IIb compounds

1.